# Direct Imaging of Exciton Transport in Tubular Porphyrin Aggregates by Ultrafast Microscopy

Yan Wan,[1#] Anna Stradomska,[2#] Jasper Knoester,[3*] and Libai Huang[1*]

[1]Department of Chemistry, Purdue University, West Lafayette, IN 47907, USA
[2]School of Chemistry, University of Glasgow, University Avenue, Glasgow, G12 8QQ, United Kingdom.
[3]Zernike Institute for Advanced Materials, University of Groningen, Nijenborgh 4, 9747AG Groningen, The Netherlands

[*] Corresponding authors: j.knoester@rug.nl, libai-huang@purdue.edu,
#: Equal contribution

**Abstract**

Long-range exciton transport is a key challenge in achieving efficient solar energy harvesting in both organic solar cells and photosynthetic systems. Self-assembled molecular aggregates provide the potential for attaining long-range exciton transport through strong intermolecular coupling. However, there currently lacks an experimental tool to directly characterize exciton transport in space and in time to elucidate mechanisms. Here we report a direct visualization of exciton diffusion in tubular molecular aggregates by transient absorption microscopy with ~ 200 fs time resolution and ~ 50 nm spatial precision. These direct measurements provide exciton diffusion constants of 3-6 $cm^2s^{-1}$ for the tubular molecular aggregates, which are 3-5 times higher than a theoretical lower bound obtained by assuming incoherent hopping. These results suggest that coherent effects play a role; despite the fact that exciton states near the band bottom crucial for transport are only weakly delocalized (over < 10 molecules). The methods presented here establish a direct approach for unraveling the mechanisms and main parameters underlying exciton transport in large molecular assemblies.

**Keywords**: Tubular aggregates, Exciton delocalization, Pump-probe microscopy

## Introduction

Long-range excitation energy transport is crucial for achieving efficient solar energy harvesting in systems such as organic solar cells and photosynthetic antennas.[1-4] Supramolecular aggregates formed by self-assembled dye molecules are among the most promising constructs for efficient excitation energy transport, because they offer the potential to control coherent and incoherent motions through modulating intermolecular coupling.[5,6] The Frenkel exciton, a collective excitation shared by many molecules, is a good description of the charge-neutral excited states of these molecular aggregates.[7] Very recently, micrometer long exciton transport has been visualized by photoluminescence (PL) microscopy in one-dimensional H-aggregate molecular fibers at room temperature, where transport is postulated to be predominantly coherent.[8] Such long-range exciton transport in molecular assemblies is remarkable because it demonstrates that macroscopic transport, which had previously only been accomplished in highly ordered organic crystals[9], is also achievable in lower dimensional aggregates by controlling intermolecular coupling. Long-range exciton migration in tubular carbocyanine dye aggregates has also been reported recently.[10,11]

Excitation energy transport is well understood theoretically at the extreme incoherent (weak) and coherent (strong) coupling limits, but is much less well understood in the intermediate regime where many molecular aggregates and photosynthetic antennas belong. Excitation energy transport in the intermediate regime has mixed coherent and incoherent characteristics.[12-14] In the intermediate regime, excitons are delocalized over part of the system and the exciton delocalization length is defined by the competition between intermolecular coupling strength and disorder. [15,16] Delocalized excitons can in principle accelerate energy transfer as compared to completely incoherent Förster hopping, because the delocalization size defines an effective hopping length that can be much larger than the nearest-neighbor intermolecular spacings.[14,17,18]

Despite the success of constructing supramolecular structures[19] for solar energy harvesting and the recent observations of long-range energy transport[8,10,11] in molecular aggregates, understanding of excitation energy transport in these structures is far from complete. To elucidate mechanisms, measurements to provide quantitative results on length and time scales of transport connected with exciton delocalization are necessary. One major challenge in measuring exciton transport in molecular aggregates lies in the requirement of simultaneous ultrafast temporal resolution and nanoscale spatial resolution, imposed by the combination of fast energy transfer (typically $\leq$ 1 ps) and short exciton diffusion lengths (typically $\leq$ 100 nm). Steady-state and time-resolved PL microscopy have been able to image the extent of exciton transport.[8,10,20-23] However, a major drawback for PL based techniques is that the time resolution is on the order of ~ 100 ps. Two of us recently developed ultrafast transient absorption microscopy as a means to directly image exciton transport with ~ 200 fs time resolution and ~ 50 nm spatial precision.[24-26] With this approach, exciton diffusion in single crystalline tetracene[24] and quantum dot superlattices[26] have successfully been visualized.

Here we report on the direct visualization of exciton diffusion in tubular molecular aggregates derived from meso-tetra(4-sulfonatophenyl) porphyrin (TPPS4) by ultrafast transient absorption microscopy. The optical properties and dynamics of excitons in self-assembled tubular molecular aggregates of a variety of natural and synthetic dye molecules have received much attention over recent years,[27-33] in particular in the context of (artificial) light-harvesting. As tubular molecular aggregates may sustain anomalously large exciton delocalization sizes,[5] these systems hold the potential for large diffusion constants and they may provide a means of assessing models for transport that interpolate between coherent and incoherent mechanisms. The experiments reported here provide direct measurements of exciton diffusion constants yielding values of 3-6 $cm^2s^{-1}$ for TPPS4 nanotubes by mapping

exciton population in space and in time. We have applied a Haken-Strobl-Reineker model[34,35] to obtain a lower bound for the exciton diffusion constant assuming the exciton motion is entirely incoherent. The measured exciton diffusion constants are 3-5 times higher than this incoherent limit. Simulation shows that the states near the band bottom crucial for exciton transport are delocalized over < 10 molecules, suggesting that coherent effects play a role despite relatively weak delocalization.

**Results and discussion**

**Structure of the porphyrin nanotubes:** TPPS4 aggregates are known to be cylindrical structures with a radius of approximately 16-18 nm[36] and a length of up to several microns. They provide a biomimetic analogue of the chlorosomes of green sulfur bacteria.[37-40] Figure 1a schematically shows the geometry of a TPPS4 tubular aggregate used in this paper, where the tubular shape is obtained by rolling a 2D sheet of porphyrin molecules onto a cylindrical surface.[40,41] This structural model has been used to explain the aggregate absorption spectrum shown in Figure 1b.[42]

For unaggregated porphyrin molecules there are two dominant absorption bands: the high intensity B-band ($S_2$ excited state) and the low intensity Q-band ($S_1$ excited state). Upon aggregation, the *B* band is split into a very narrow red-shifted peak at 490 nm (2.53 eV) and a wider peak at 423 nm (2.93 eV); these two peaks originate from different B-band excitons[40,41]. The *Q* band is red-shifted upon aggregation from 647 nm to 707 nm and 675 nm. The red-shift and narrowing of the absorption spectrum are signatures of the formation of delocalized states in J aggregates. The absorption spectra of the Frenkel excitons in TPPS4 aggregates have been simulated successfully.[42]

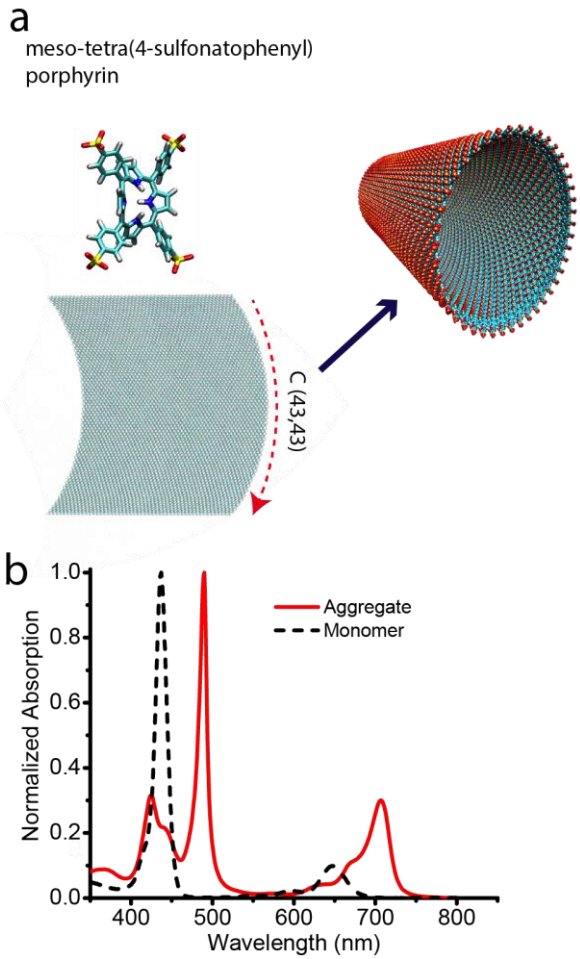


**Figure 1.** Structure of the porphyrin nanotubes. (a) Chemical structure of the meso-tetra(4-sulfonatophenyl) porphyrin (TPPS4) monomer (top). The tubular aggregate forms at pH ~ 1. In order to obtain a structural model (top), a planar aggregate (bottom) is seamlessly rolled onto the surface of a cylinder along the chiral vector C of (43,43) (in units of the lattice constants), in such a way that the chiral vector becomes the circumference of the cylinder.[41] (b) Normalized UV-vis absorption spectra of aggregate and monomer in solution at room temperature.

**Exciton dynamics in small nanotube bundles:** We perform correlated atomic force microscopy (AFM) and transient absorption microscopy (TAM) to locate porphyrin nanotubes and to measure exciton dynamics. Figure 2a shows the AFM height image of the porphyrin nanotubes deposited on a glass substrate, which confirms the formation of tubular aggregates. The nanotubes become flattened when they are deposited on a substrate as indicated by the height of ~ 4 nm for individual nanotubes measured by AFM, similar to previously reported values.[43] Small bundles may be formed by a few porphyrin nanotubes

stacking parallel to each other along their long axes as shown in more detail by AFM amplitude imaging in Figure S1 of the supporting information (SI). As reported by Rotomskis *et.al.*[43], while the TPP4 nanotubes are flattened after the deposition on glass substrates, the excitonic structure does not change significantly. The absorption spectrum of TPPS4 nanotubes deposited on glass substrates was shown to be almost identical to that of isolated nanotubes in aqueous acidic solution.[43]

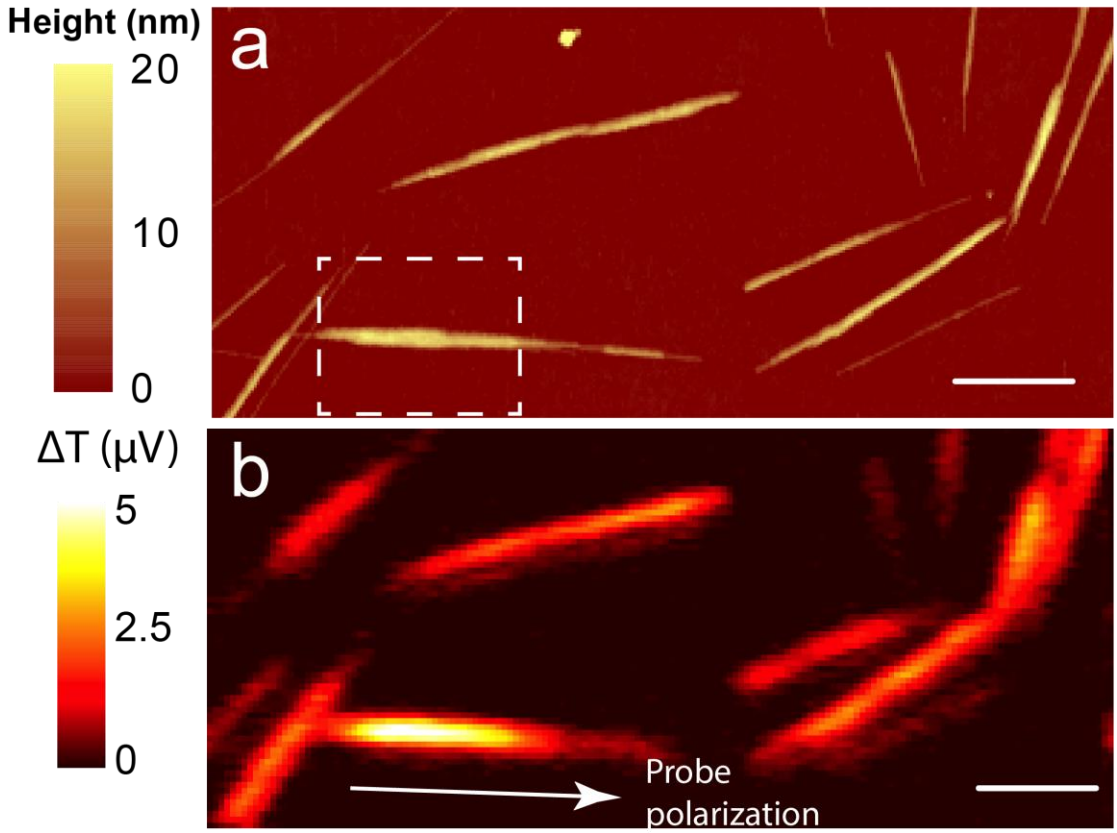


**Figure 2.** Correlated AFM-TAM measurements**.** (a) AFM height image of TPPS4 porphyrin nanotubes deposited on a glass substrate. (b) Correlated TAM image of the same sample area at 0 ps pump probe delay. Pump and probe beams are overlapped in space. The pump intensity was 4.1 μJcm$^{-2}$. Scale bar: 1μm. The rectangle in (a) marks a small bundle for the following TAM imaging of exciton transport as shown in Figure 4.

Figure 2b shows the correlated morphological TAM image taken at 0 ps pump-probe delay, of the same area as imaged by AFM in Figure 2a. In this mode of TAM imaging, the pump and probe beams are always overlapped spatially (Figure S2), a piezo stage is used to

scan the sample to construct images. Such TAM images reflect the spatial locations of the nanotubes on the substrate as shown in Figure 2. For the TAM measurements, the pump wavelength is at 396 nm, exciting the B band, while the probe wavelength is at 707 nm, probing the ground state bleach of the Q band. The pump-probe signal is proportional to the initial density of excitons and scales with the number of nanotubes in a bundle. As shown in Figure 2, a higher TAM intensity corresponds to a larger number of nanotubes in a bundle. Both the pump and the probe are linearly polarized. The transient absorption signal is strongly dependent on the probe polarization, because the Q band transition probed has a transition dipole parallel to the long axis of the nanotube.[41] Further characterization of the probe polarization dependence is shown in Figure S3. A very good correlation between AFM and TAM can be seen, demonstrating that TAM is sensitive enough to image individual porphyrin nanotubes and small bundles.

Figure 3 displays the exciton dynamics probed in a small porphyrin nanotube bundle. Exciton decay is rapid and highly nonexponential and decay constants of 3 ps, 23 ps, and 420 ps are extracted by fitting to a tri-exponential decay convoluted with a Gaussian response function, as shown in Figure 3a. To ensure that exciton-exciton annihilation does not play a role, we have carried out pump intensity dependent measurements (Figure 3b). We find negligible pump intensity dependence on the experimental range of 0.4 $\mu J/cm^2$ to 4.1 $\mu J/cm^2$ and therefore conclude that exciton-exciton annihilation is insignificant in the measurements presented here. We note that the exciton decay observed for this particular nanotube bundle is overall similar to the dynamics measured in the isolated nanotubes in solution (Figure S4).[42] Also, exciton dynamics measured in different bundles are identical, as shown in Figure S5. These observations indicate that variations in the decay between nanotubes are not very important or, in other words, that the part of the tube probed is large enough to self-average the decay characteristics.

The low quantum yield (0.002 at 3 K) indicates that nonradiative pathways dominate energy relaxation in the aggregates. In our previous work[42], the nonexponential exciton decay has been attributed to an inhomogeneous distribution of exciton states, and the few ps decay component has been ascribed to the trapping of excitons by dark (possibly disorder-induced) states. As shown in Figure S4, the dynamics in the nanotube bundles measured at 80 MHz repetition rate (12 ns between pulses) are identical to those in isolated nanotubes in solution measured at 1kHz (1 ms between pulses), indicating that long-lived triplet states do not play an important role.

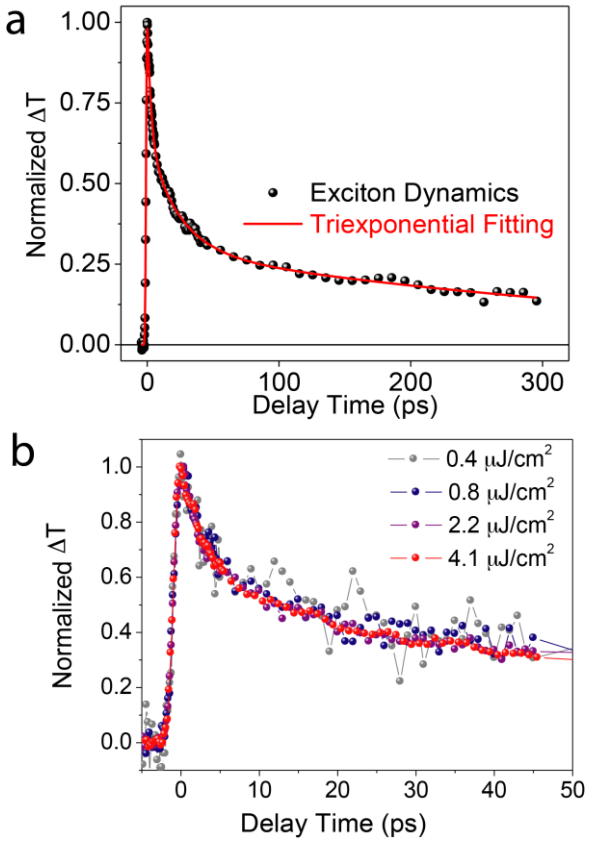


**Figure 3.** (a) Exciton dynamics measured in a small nanotube bundle fitted with a tri-exponential decay function convoluted with a Gaussian response function. The pump intensity was 4.1 μJ/cm$^2$ (b) Exciton dynamics measured at different pump intensities as labeled.

**Direct imaging of exciton propagation:** To image exciton transport, a new mode of TAM is

employed in which the pump beam is held at a fixed position, while the probe beam is spatially scanned relative to the pump with a Galvanometer scanner to form an image (Figure S2).[25] In the experiments reported here, the location of the pump beam is fixed at the center of a small bundle as marked by the rectangle in Figure 2a. The probe polarization is set to be parallel to the porphyrin nanotube bundle. Figure 4a illustrates the exciton population at 0, 3, and 15 ps pump-probe delay times. In these TAM images, the spatial distribution of exciton population as a function of pump-probe delay is directly visualized. At 0 ps, the TAM image represents the initial exciton population created by the pump beam. At later delay times, the TAM images reflect the range of exciton migration from the initial excitation volume.

To correctly measure exciton transport, it is important to understand how exciton-exciton annihilation processes influence the spatial distribution of the excitons under the experimental conditions used. Because the exciton density at the center of the spot is higher than near the edge, exciton-exciton annihilation could lead to artificial broadening of the exciton distribution, as it would cause a faster exciton decay near the center. As shown in Figure 3, exciton-exciton annihilation is negligible at the pump intensity of 4.1 $\mu J/cm^2$ (~1 exciton/ 1000 molecules) used for the transport measurements.

The exciton density profiles along the long axis of the porphyrin nanotube bundle at different pump-probe delay times fitted with Gaussian functions are shown in Figure 4b. The exciton profile broadens as the pump probe delay time increases along the long axis, reflecting the transport of excitons out of the initial excitation volume. In contrast, the profiles along the short axis do not change as a function of the pump-probe delay (Figure S6). We have also performed a control experiment on a conjugated polymer thin film where excitons diffuse < 2 nm in the 15 ps time window and no time-dependence in the exciton

density profile was observed in that case (Figure S7), confirming that the broadening seen in Figure 4b is indeed due to exciton diffusion in the porphyrin nanotube bundle.

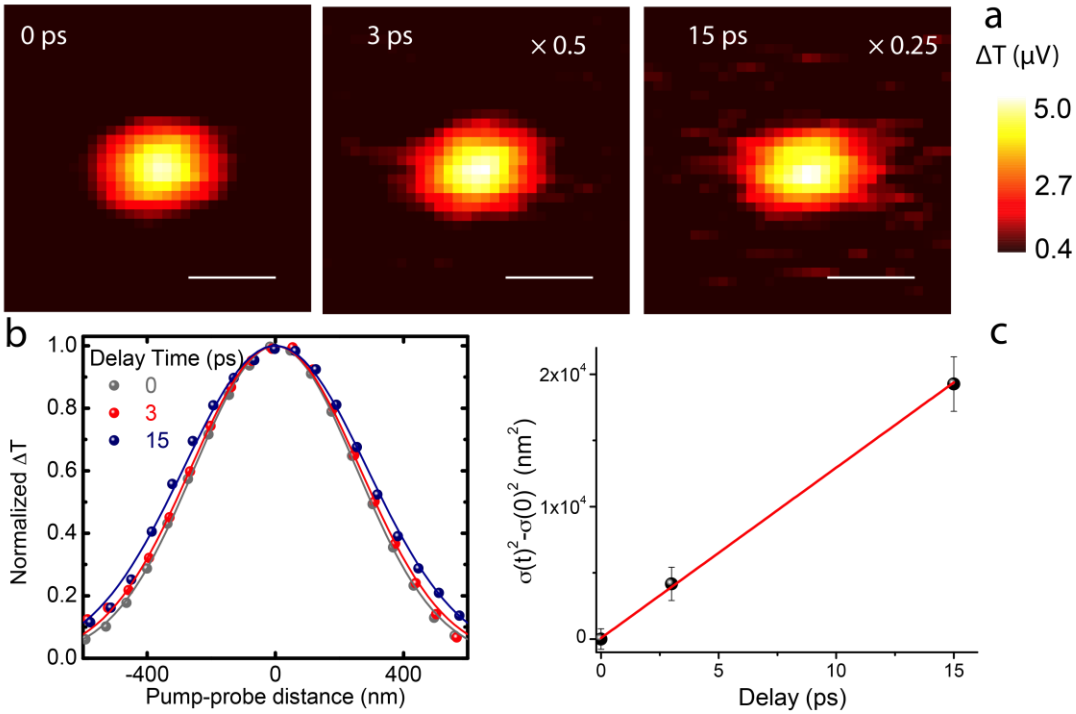


**Figure 4.** TAM imaging of exciton transport. (a) TAM images of exciton propagation at different pump-probe delay times for the bundle of nanotubes as marked in Figure 2a. The color scale represents the intensity of the differential transmission (ΔT) of the probe beam at 0 ps. For 3 and 15 ps, ΔT is plotted on relative scales to the one at 0 ps, with the multiplication factor as labeled. The images show the spatial distribution of the ΔT signal measured at pump-probe delay times as labeled. Scale bar: 0.5 μm. The pump intensity was 4.1 μJ/cm$^2$. (b) Cross-sections of the TAM images along the long axis fitted with Gaussian functions at different delay times with the maximum ΔT signal normalized to unity. (c) $\sigma_t^2 - \sigma_0^2$ as a function of pump-probe delay time (symbols), with a linear fit to equation 4 (line), which yields a diffusion constant of 6.4 ± 0.2 cm$^2$s$^{-1}$. Error bars of $\sigma_t^2 - \sigma_0^2$ are the standard errors estimated from Gaussian fitting to the spatial intensity distributions.

To analyze the observed exciton transport along the axis of the nanotube, we consider a description in the diffusive limit, which is governed by a phenomenological diffusion equation for the exciton density that includes decay to the ground state:

$$\frac{\partial\, n(x,t)}{\partial t} = D\,\frac{\partial\, n^2(x,t)}{\partial x^2} - \frac{n(x,t)}{\tau} \qquad (1)$$

Here $n(x,t)$ is the exciton density as a function of position and time, $D$ is the diffusion constant, and $\tau$ is the exciton lifetime. The initial exciton density profile at time zero,

$n(x,0)$, is a 1D Gaussian distribution with a variance of $\sigma_0^2$ created by a Gaussian pump beam at position $x_0$ along the tube, as given by $n(x,0) = Nexp(-\frac{(x-x_0)^2}{2\sigma_0^2})$, where $N$ is a constant determined by the laser intensity and the absorbance of the tube. The solution to equation 1 shows that the density profile at any later time $t$ is also Gaussian, $n(x,t) = Nexp(-\frac{(x-x_0)^2}{2\sigma_t^2})$, with a variance $\sigma_t^2$ given by $\sigma_t^2 = \sigma_0^2 + 2Dt$. Thus, a linear fit of the measured Gaussian variance as a function of time directly yields the diffusion constant as half of the slope as given by,

$$D = \frac{\sigma_t^2 - \sigma_0^2}{2t} \qquad (2)$$

The measured profile along the tube axis is convoluted with the profiles of the pump and probe beams, which have width of 228 nm and 287 nm, respectively (Figure S8). Because both beam profiles are Gaussian with widths that do not change over the pump-probe delay time, this merely results in replacing $\sigma_0^2$ by $\sigma_0^2 + \sigma_{pump}^2 + \sigma_{probe}^2$ (with the $\sigma_{pump}^2$and $\sigma_{probe}^2$ indicating the variances of the laser profiles) and hence not affecting the linear dependence on $t$ and the extraction of $D$ from the measurements. $\sigma_0$ and $\sigma_t$ are extracted from the Gaussian fits as shown in Figure 4b. The precision in determining the exciton propagation distance is dictated by the smallest measurable change in the excited state population profile, and not directly by the diffraction limit. For the signal-to-noise levels shown in Figure 4, this limit is ~ 50 nm for the current experimental conditions. More details on the signal-to-noise limit and the ability to resolve diffusion can be found in the SI.

The evolution of $\sigma_t^2 - \sigma_0^2$ as a function of pump-probe delay time is plotted in Figure 4c. Although the number of data points is limited, Figure 4c suggests a linear dependence of $\sigma_t^2 - \sigma_0^2$ on the pump-probe delay time, indicative of diffusive exciton transport on the relevant time scale. A linear fit to the data then yields the diffusion $D$ using equation (2). The

fit yields $D$ = 6.4 ± 0.2 $cm^2s^{-1}$ for the particular bundle of tubes imaged in Figure 4. The TAM results for two other bundles of nanotubes are shown in Figures S9 and S10, from which diffusion constants of 3.0 ± 0.2 and 5.4 ± 2.3 $cm^2s^{-1}$, respectively, are obtained. These diffusion constants are similar in magnitude to the diffusion constant of 1.2 $cm^2s^{-1}$ estimated for the carbocyanine dye nanotubes from steady-state PL microscopy measurements.[10]

**Simulation of the exciton diffusion constant**: Since, by fitting the absorption and linear dichroism spectra of TPPS4 nanotubes in our previous work,[42] we have already built a microscopic model for the excitons and their dynamics, it is useful to see whether this model predicts a long-time diffusion constant similar to the TAM measurements. This microscopic model is characterized by a Frenkel exciton Hamiltonian in which the four molecular electronic transitions ($Q_x$, $Q_y$, $B_x$, and $B_y$) are mutually coupled by intermolecular excitation transfer (dipole-dipole) interactions $J_{nj,ml}$, where $n$ and $m$ denote the two molecules that are coupled and $j$ and $l$ the respective excited states of these molecules involved in the coupling. Furthermore, the model includes static disorder in the molecular transition energies and linear coupling (Holstein type) between the electronic excitations and an intramolecular vibrational mode. The model Hamiltonian is given in the Methods section (equation 4); its parametrization is taken from Ref. 31. Finally, in order to describe the dynamics, coupling of the vibronic states to a heat bath is included and treated perturbatively, in exactly the same way as in Ref. 31.

To model the exciton transport, in addition to the intermolecular transfer interactions $J_{nj,ml}$, the exciton dephasing rate $\Gamma$ is essential (see below). The latter, we may replace by the homogeneous linewidth of the excitons, which we also have obtained from our previous modeling.[42] We neglect interactions between different nanotubes that make up the bundles on which the measurements were done, thus assuming that the exciton transport within the

bundles is dominated by transport within a single nanotube. Such treatment is justified, because the absorption spectrum of TPPS4 nanotube bundles flattened on a glass substrate is almost identical to that of the isolated nanotubes in solution (no shifting of the J band)[43], indicating that intertube interaction in the TPPS4 bundles is negligible.

In order to estimate the exciton diffusion constant, we use the Haken-Strobl-Reineker (HSR) model[34,44] which is a white-noise model that has been used frequently to model exciton transport. Assuming the limit where dephasing has rendered the transport process an entirely incoherent hopping process between individual molecules, the transport is diffusive and within the HSR model a simple expression can be obtained for the diffusion tensor.[34] In order to apply this approach to TPPS4 nanotubes, we generalize the original HSR model to account for multiple electronic excited states per molecule; furthermore we disregard the non-local coupling between the excitons and the bath, in accordance with the model Hamiltonian (4). This leads to the equation for the diffusion tensor $D$ in the form of

$$D_{\alpha\beta} = \frac{1}{2\hbar\Gamma}\sum_{m\neq 0}\sum_{j,l}\left(J_{0j,ml}\right)^2 X_{m\alpha}X_{m\beta} \qquad (3)$$

where $\alpha$ and $\beta$ denote the Cartesian components ($x$, $y$, $z$), $\Gamma$ is the homogeneous linewidth, $m$ numbers the molecules within the aggregate (molecule 0 denoting a central molecule), the summations over $j$ and $l$ run over the relevant molecular electronic excited states, and $X_{m\alpha}$ is the $\alpha$th Cartesian component of the lattice vector of molecule $m$ relative to the central molecule. Because of the fast relaxation (~ 300 fs) of the B-band excitons into the Q-band,[45] only the Q-band states directly contribute to exciton diffusion at timescales studied here. Thus, the summation over $j$ and $l$ in equation (3) is taken to only run over the $Q_x$ and $Q_y$ states. We carried the summation over the molecules $m$ until convergence was reached.

The lattice vectors were calculated based on our model of the aggregate geometry (see Ref.[41]), and the resonance integrals $J_{0j,ml}$ were obtained using the extended dipole

approximation that we previously employed in our modeling of optical spectra of TPPS4 nanotubes.[41,42] The Haken-Strobl-Reineker model assumes that one value of the homogeneous linewidth is applicable for the whole exciton band. In reality, this linewidth, which is dominated by intraband scattering, depends on the energy of the exciton and generally increases with increasing energy. We have found this energy-dependent width in our previous modeling of the spectroscopy of TPPS4 nanotube, and the plot can be found as Figure S9 in the SI. In order to provide a single value for the modeling of the diffusion coefficient, we have chosen to use a value of $\Gamma$ = 0.014 eV, obtained as the average homogeneous linewidth over the whole *Q* band and over all 200 disorder realizations studied.

As a result, we obtain a theoretical estimate for the diffusion constant along the axis of a porphyrin nanotube of 1.20 $cm^2s^{-1}$, a factor of 2.5-5.3 times smaller than the experimentally obtained values. Because the nanotubes become flattened when deposited, we have also simulated the diffusion constant in a planar aggregate. The diffusion constant in a planar aggregate is 1.18 $cm^2s^{-1}$, almost identical to that of a perfect tube. The morphological deformations have relatively small effects on exciton diffusion, because the diffusion constant is determined mostly by the interactions with a small number of nearest neighbors. Specifically, in case of diffusion along the TPPS4 tube axis, 82% of the simulated diffusion constant comes from interactions with the 4 nearest neighbors and the 2 next-nearest neighbors that are located along the tube direction, which do not change significantly when the tube is flattened.

Given the approximations made above, the simulated diffusion constant is in a reasonable agreement with the experiments. It is interesting to question whether the underestimation of the diffusion constant in our simulation results from the neglect of exciton delocalization in the above approach. As argued in the Introduction, one generally expects

exciton delocalization (i.e. quantum coherent effects) to lead to a larger diffusion constant. Interestingly, such effects may be accounted for in the Haken-Strobl-Reineker model by starting from a more general point of view, in which the diffusion constant is obtained via the two-time correlation function of the flux operator that describes energy transport.[18] In order to numerically implement this for the large tubular aggregates involved, approximations need to be made (such as the use of one average homogeneous linewidth), which make it questionable how meaningful this more elaborate calculation would be. We, therefore, have refrained from investigating this more sophisticated implementation of the HSR model for our particular aggregates. Instead, we have studied the delocalization of the excitons in more detail, so as to be able to judge whether the neglect of delocalization in the calculation of the diffusion constant is reasonable or not.

**Simulation of exciton delocalization:** In order to quantify the exciton delocalization size, we account for the competition between excitation transfer interactions and static disorder in TPPS4 tubes, as well as the linear coupling of excitons to one vibrational mode, as incorporated in Hamiltonian. We generalize the definition of the participation ratio[15,46] for vibronic eigenstates:

$$PR(\varphi_k) = \sum_{n,j} |\langle \varphi_k | nj \rangle \langle nj | \varphi_k \rangle|^2 \qquad (4)$$

where $\varphi_k$ is the state of interest, $|nj\rangle$ denotes a state with molecule $n$ in its $j$th electronic excited state (see Methods section in the SI). Such generalization of the participation ratio retains the properties of the original definition: a state completely localized on a single molecule yields a participation ratio of one, while a state uniformly delocalized over *N* molecules results in a participation ratio of *N*.

We obtained data on the exciton delocalization by averaging the results of a series of calculations performed for 200 random realizations of the static disorder $\Delta_{nj}$. For the

optically dominant states within the Q-band the average participation ratio (delocalization number) is 208 ± 152 molecules, while at the absorption maximum of the lower component of the B-band it reaches 1036 ± 224 molecules.

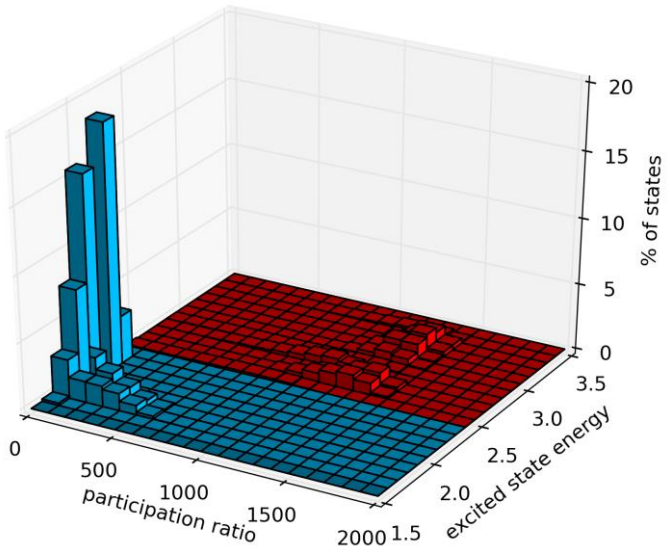


**Figure 5**. Energy resolved distribution of the exciton participation ratio. The Q-band excitons are marked in blue, the B-band excitons are marked in red.

The details of the distribution of exciton participation ratios per exciton energy interval are shown in Figure 5. The delocalization of the B band states is large: in the whole B band merely 0.01% of the states is localized on less than 10 molecules, and 80% is delocalized over 1000-1500 molecules. Because there are 43 molecules around the tube's circumference, the B band is initially delocalized over ~ 25 rings (16.5 nm along the tube axis) assuming the exciton is distributed fully around the tube. Through fast relaxation from the B to the Q band (within the pulse width of ~ 200 fs), this delocalization will contribute ~ 16.5 nm to the initial broadening of the exciton profile included in the initial distribution $\sigma_0$ and does not play a role in the diffusion constant deduced from the time dependence of $\sigma_t^2 - \sigma_0^2$.

We also observe that, even though for the Q-band the delocalization of the optically dominant states is large, it turns out that the majority of Q-band excitons is delocalized over a

small number of molecules: 65.1% of the states is delocalized over less than 5 molecules, and 71.9% over less than 10 molecules. The localization is even stronger close to the band bottom: in the low-energy tail of the density of states below 1.68 eV all excitons are localized on less than 5 molecules, while within the range *kT* above 1.68 eV 91.3% of the excited states is localized on less than 5 molecules, while 99.5% is localized on less than 10 molecules (Figure S11). These states, which evidently are only weakly delocalized, are the ones that are crucial for the exciton transport. This offers a possible explanation why the result obtained from our simple incoherent implementation (equation 3) of the Haken-Strobl-Reineker model for the diffusion constant still provides a correct order of magnitude estimate of the measured value.

**Conclusions**

In summary, we have demonstrated transient absorption microscopy as a means to directly measure exciton transport in tubular porphyrin aggregates in space and in time. The excitons in tubular aggregates provide a model for evaluating transport in quasi-one-dimensional systems, whose exciton delocalization size is enhanced by the locally two-dimensional nature of the system in combination with the long-range (dipolar) interactions.[5] We have measured exciton diffusion constants of 3-6 $cm^2s^{-1}$ in tubular TPPS4 aggregates, 3-5 times higher than the lower bound incoherent hopping limit, suggesting that coherent effects may play a role, albeit that they do not lead to a huge enhancement. Simulation shows that the states near the band bottom crucial for exciton transport are weakly delocalized (over < 10 molecules), which is consistent with the absence of a very large enhancement of the diffusion constant. It will be of interest to study other systems with our methods, where exciton delocalization for the states dominant in transport are more pronounced. For instance, recent exciton-exciton annihilation measurements in strongly-coupled cyanine dye aggregates suggest an exciton diffusion constant as high as 50 $cm^2s^{-1}$.[11] In general, the spatially- and

temporally-resolved measurements reported here establish a significant step toward discerning the underlying excitation energy transport mechanisms in supramolecular aggregates.

ASSOCIATED CONTENT: Supporting Information describes sample preparation, factors that control spatial resolution of transient absorption microscopy, and supplemental figures. Supporting Information is available free of charge *via* the internet at http://pubs.acs.org.

ACKNOWLEDGMENTS

L.H. and Y.W. acknowledge support from US National Science Foundation through grant NSF-CHE-1555005.

**References:**

(1) Blankenship, R. E.; Tiede, D. M.; Barber, J.; Brudvig, G. W.; Fleming, G.; Ghirardi, M.; Gunner, M. R.; Junge, W.; Kramer, D. M.; Melis, A.; Moore, T. A.; Moser, C. C.; Nocera, D. G.; Nozik, A. J.; Ort, D. R.; Parson, W. W.; Prince, R. C.; Sayre, R. T. *Science* **2011**, *332*, 805-809.
(2) Fleming, G. R.; Schlau-Cohen, G. S.; Amarnath, K.; Zaks, J. *Farad. Discuss.* **2012**, *155*, 27-41.
(3) Scholes, G. D.; Fleming, G. R.; Olaya-Castro, A.; Van Grondelle, R. *Nat. Chem.* **2011**, *3*, 763-774.
(4) Menke, S. M.; Luhman, W. A.; Holmes, R. J. *Nat. Mater.* **2013**, *12*, 152-157.
(5) Bloemsma, E. A.; Vlaming, S. M.; Malyshev, V. A.; Knoester, J. *Phys. Rev. Lett.* **2015**, *114*, 156804.
(6) Yuen-Zhou, J.; Saikin, S. K.; Yao, N. Y.; Aspuru-Guzik, A. *Nat. Mater.* **2014**, *13*, 1026-1032.
(7) Főrster, T. *Discuss. Faraday Soc.* **1959**, *27*, 7-17.
(8) Haedler, A. T.; Kreger, K.; Issac, A.; Wittmann, B.; Kivala, M.; Hammer, N.; Köhler, J.; Schmidt, H.-W.; Hildner, R. *Nature* **2015**, *523*, 196-199.
(9) Ern, V.; Avakian, P.; Merrifield, R. *Phys. Rev.* **1966**, *148*, 862.
(10) Clark, K. A.; Krueger, E. L.; Vanden Bout, D. A. *J. Phys. Chem. Lett.* **2014**, *5*, 2274-2282.
(11) Caram, J. R.; Doria, S.; Eisele, D. M.; Freyria, F. S.; Sinclair, T. S.; Rebentrost, P.; Lloyd, S.; Bawendi, M. G. *Nano Lett.* **2016**, *16*, 6808-6815.
(12) Jang, S.; Newton, M.; Silbey, R. *Phys. Rev. Lett.* **2004**, *92*, 218301.
(13) Beljonne, D.; Curutchet, C.; Scholes, G. D.; Silbey, R. J. *J. Phys. Chem. B* **2009**, *113*, 6583-6599.
(14) Fujita, T.; Brookes, J. C.; Saikin, S. K.; Aspuru-Guzik, A. *J. Phys. Chem. Lett.* **2012**, *3*, 2357-2361.
(15) Fidder, H.; Knoester, J.; Wiersma, D. A. *J. Chem. Phys.* **1991**, *95*, 7880-7890.
(16) Schreiber, M.; Toyozawa, Y. *J. Phys. Soc. Jpn.* **1982**, *51*, 1528-1536.
(17) Lloyd, S.; Mohseni, M. *New J. Phys.* **2010**, *12*, 075020.
(18) Chuang, C.; Lee, C. K.; Moix, J. M.; Knoester, J.; Cao, J. *Phys. Rev. Lett.* **2016**, *116*, 196803.
(19) Sengupta, S.; Wurthner, F. *Acc. Chem. Res.* **2013**, *46*, 2498-2512.
(20) Snoke, D.; Denev, S.; Liu, Y.; Pfeiffer, L.; West, K. *Nature* **2002**, *418*, 754-757.

(21) Akselrod, G. M.; Deotare, P. B.; Thompson, N. J.; Lee, J.; Tisdale, W. A.; Baldo, M. A.; Menon, V. M.; Bulović, V. *Nat. Commun.* **2014**, *5*, 3646.
(22) Irkhin, P.; Biaggio, I. *Phys. Rev. Lett.* **2011**, *107*, 017402.
(23) Najafov, H.; Lee, B.; Zhou, Q.; Feldman, L.; Podzorov *Nat. Mater.* **2010**, *9*, 938-943.
(24) Wan, Y.; Guo, Z.; Zhu, T.; Yan, S.; Johnson, J.; Huang, L. *Nat. Chem.* **2015**, *7*, 785-792.
(25) Guo, Z.; Manser, J. S.; Wan, Y.; Kamat, P. V.; Huang, L. *Nat. Commun.* **2015**, *6*, 7471.
(26) Yoon, S. J.; Guo, Z.; dos Santos Claro, P. C.; Shevchenko, E. V.; Huang, L. *Acs Nano* **2016**, *10*, 7208-7215.
(27) Spitz, C.; Knoester, J.; Ouart, A.; Daehne, S. *Chemical Physics* **2002**, *275*, 271-284.
(28) Lang, E.; Sorokin, A.; Drechsler, M.; Yuri V Malyukin, a.; Köhler, J. *Nano Lett.* **2005**, *5*, 2635-2640.
(29) Ganapathy, S.; Oostergetel, G. T.; Wawrzyniak, P. K.; Reus, M.; Gomez Maqueo Chew, A.; Buda, F.; Boekema, E. J.; Bryant, D. A.; Holzwarth, A. R.; de Groot, H. J. M. *Proc. Natl. Acad. Sci. U.S.A.* **2009**, *106*, 8525-8530.
(30) Günther, L. M.; Jendrny, M.; Bloemsma, E. A.; Tank, M.; Oostergetel, G. T.; Bryant, D. A.; Knoester, J.; Köhler, J. *J. Phys. Chem. B* **2016**, *120*, 5367-5376.
(31) Eisele, D. M.; Cone, C. W.; Bloemsma, E. A.; Vlaming, S. M.; van der Kwaak, C. G. F.; Silbey, R. J.; Bawendi, M. G.; Knoester, J.; Rabe, J. P.; Bout, D. A. V. *Nat. Chem.* **2012**, *4*, 655-662.
(32) Abramavicius, D.; Nemeth, A.; Milota, F.; Sperling, J.; Mukamel, S.; Kauffmann, H. F. *Phys. Rev. Lett.* **2012**, *108*, 067401.
(33) Sengupta, S.; Ebeling, D.; Patwardhan, S.; Zhang, X.; von Berlepsch, H.; Böttcher, C.; Stepanenko, V.; Uemura, S.; Hentschel, C.; Fuchs, H.; Grozema, F. C.; Siebbeles, L. D. A.; Holzwarth, A. R.; Chi, L.; Würthner, F. *Angew. Chem. Int. Ed.* **2012**, *51*, 6378-6382.
(34) Haken, H.; Reineker, P. *Acta Universitatis Carolinae. Mathematica et Physica* **1973**, *14*, 23-47.
(35) Haken, H.; Strobl, G. *Zeitschrift fr Physik* **1973**, *262*, 135-148.
(36) Short, J. M.; Berriman, J. A.; Kübel, C.; El-Hachemi, Z.; Naubron, J.-V.; Balaban, T. S. *Chemphyschem* **2013**, *14*, 3209-3214.
(37) Shibata, Y.; Tateishi, S.; Nakabayashi, S.; Itoh, S.; Tamiaki, H. *Biochemistry* **2010**, *49*, 7504-7515.
(38) Orf, G. S.; Blankenship, R. E. *Photosynthesis Research* **2013**, *116*, 315-331.
(39) Hollingsworth, J. V.; Richard, A. J.; Vicente, M. G. H.; Russo, P. S. *Biomacromolecules* **2012**, *13*, 60-72.
(40) Vlaming, S. M.; Augulis, R.; Stuart, M. C. A.; Knoester, J.; van Loosdrecht, P. H. M. *J. Phys. Chem. B* **2009**, *113*, 2273-2283.
(41) Stradomska, A.; Knoester, J. *J. Chem. Phys.* **2010**, *133*, 094701.
(42) Wan, Y.; Stradomska, A.; Fong, S.; Guo, Z.; Schaller, R. D.; Wiederrecht, G. P.; Knoester, J.; Huang, L. *J. Phys. Chem. C* **2014**, *118*, 24854-24865.
(43) Rotomskis, R.; Augulis, R.; Snitka, V.; Valiokas, R.; Liedberg, B. *J. Phys. Chem. B* **2004**, *108*, 2833-2838.
(44) Reineker, P. In *Exciton Dynamics in Molecular Crystals and Aggregates*; Springer Berlin Heidelberg: Berlin, Heidelberg, 1982, p 111-226.
(45) Kano, H.; Kobayashi, T. *J. Chem. Phys.* **2002**, *116*, 184.
(46) Thouless, D. J. *Phys. Rep.* **1974**, *13*, 93-142.

**TOC**